COMPDYN 2011
3rd ECCOMAS Thematic Conference on
Computational Methods in Structural Dynamics and Earthquake Engineering
M. Papadrakakis, M. Fragiadakis, V. Plevris (eds.)
Corfu, Greece, 25–28 May 2011

NEGATIVE STIFFNESS DEVICE FOR SEISMIC PROTECTION OF STRUCTURES – AN ANALYTICAL AND EXPERIMENTAL STUDY

Apostolos A. Sarlis[1], Dharma Theja R. Pasala[2], Michael C. Constantinou[1], Andrei M. Reinhorn[1], Satish Nagarajaiah[2] and Douglas Taylor[3]

[1]State University of New York at Buffalo, Buffalo, NY-14260, U.S.A
{aasarlis,constan1,reinhorn}@buffalo.edu

[2]Rice University, Houston, TX-77005, U.S.A
{drp1, Satish.Nagarajaiah}@rice.edu

[3]Taylor Devices Inc., North Tonawanda, NY-14120, U.S.A
TaylorDevi@aol.com

Keywords: Negative Stiffness Device, Apparent yielding, Passive, True Negative Stiffness

Abstract. *Structural weakening and damping is an approach previously proposed for the reduction of seismic forces and drifts in structures. While this approach is very efficient, it requires a reduction in strength, which will result in inelastic excursions and permanent deformation of the structural system during the seismic event. This paper describes a true Negative Stiffness Device (NSD) that can emulate weakening of the structural system without inelastic excursions and permanent deformations. The Negative Stiffness Device (NSD) is a self contained device that produces a force which is in the same direction as the imposed displacement, thus the name "negative stiffness". The device is inherently unstable but when installed in a structure transfers a force at its installation level which in turn reduces all forces, drifts and accelerations above that level. The NSD is therefore capable of limiting the forces developed in a structure without any yielding which could lead to permanent deformations. The NSD was developed at the University at Buffalo (UB), Rice University and Taylor Devices Inc. and tested on a shake table by authors in a three storied structural model isolated with elastomeric bearings. The NSD consists of a highly compressed spring in a double negative stiffness magnification mechanism. In order to ensure a considerable amount of positive stiffness of the global system around small displacements to minimize wind vibrations a so called gap spring assembly (GSA) mechanism is implemented which delays the engagement of the device by a prescribed displacement. Moreover, the device employs double containment chevron braces that contain the large vertical forces needed for the development of negative stiffness without transferring these forces to the structure. This paper describes the development of analytical and computational tools that describe the behavior of the device and presents results for the experimental verification of these tools.*

1 INTRODUCTION

Designing structures for ductile behavior and allowing for significant inelastic action in strong earthquakes results in reduction of inertia forces. However, this is accompanied by large drifts, permanent deformations and eventually loss of functionality of the structure after a seismic event. Reinhorn et al. (2005) [1] and Viti et al. (2006) [2] introduced the concept of weakening structures (reducing strength and implicitly stiffness), while introducing supplementary viscous damping to reduce simultaneously total accelerations and inter-story drifts. However, weakening also reduces strength and results in some permanent displacements. An alternative approach is to "simulate yielding" by introducing negative stiffness at predescribed displacements leading to the idea of "apparent weakening".

The concept of true negative stiffness for structural applications was first introduced by Nagarajaiah et al [3]. True negative stiffness means the force must assist motion, not oppose it as it is in the case of a positive stiffness spring. Pseudo negative stiffness [4] can be accomplished using active or semiactive hydraulic device. True negative stiffness needs no external power supply. The Negative Stiffness Device (NSD) presented herein is entirely composed of springs and generates an elastic nonlinear true negative stiffness.

By engaging the NSD at an appropriate displacement (simulated yield displacement), which is well below the actual yield displacement of the structural system, the composite structure-device assembly, behaves like a yielding structure. The NSD has a re-centering mechanism thereby avoiding permanent deformation in the composite structure-device assembly unless, the main structure itself yields. However, the combined structural system with just the NSD develops increased structural deformations. Addition of passive dampers reduces and controls these deformations without any considerable increase in the base shear. The addition of dampers combined with the reduction of stiffness also lead to an increased damping ratio which presents an additional advantage in controlling the displacements.

In order to visualize the effect of adding true negative stiffness to a structure, consider the force displacement plots shown in Figure 1(a) (green line is structure, magenta is viscous damper and red is negative stiffness device). By adding NSD to the structure, schematically shown in Figure 1(b), the assembly stiffness reduces to $K_a = K_e - K_n$ beyond the displacement x_1 (shown as blue line in Figure 1(b)). If, F_2 and x_2 are the maximum restoring force and maximum displacement of a perfectly-linear system (green line in Figure 1(b)) then for the same load the maximum restoring force and maximum displacement of the assembly are F_3 and x_3 (blue line in Figure 1(b)), respectively. K_n is designed to achieve the desired reduction in base shear. Force exerted by the NSD is shown as red line in Figure 1(b). Although the reduction in base shear is achieved the maximum deformation of the adaptive system is substantially increased in the process when compared with an elastic system. Deformation of this assembly can be reduced by adding a passive damping device in parallel to the NSD, schematically shown in Figure 1(c).

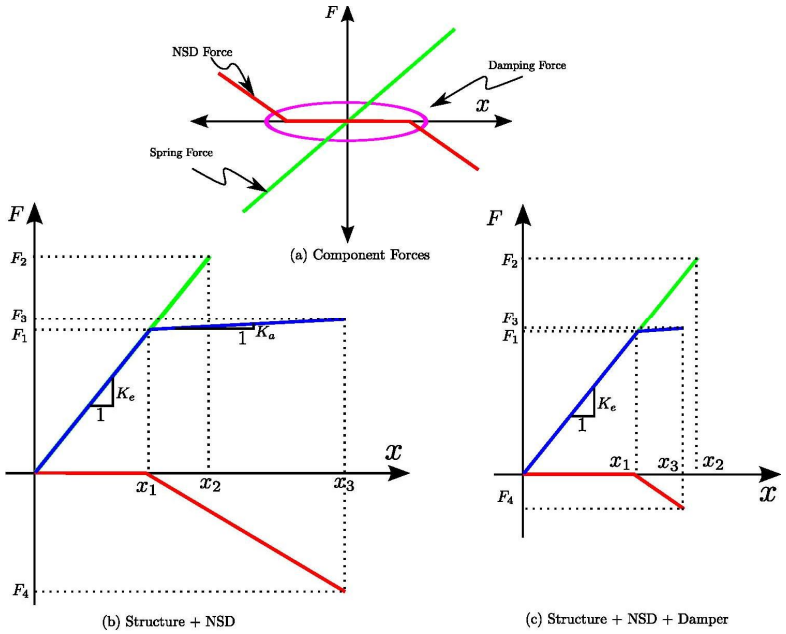

Figure 1: Working Principle of NSD (Nagarajaiah et al 2010)

Photographs of the NSD are shown in Figure 2a (un-deformed) and Figure 2b (deformed). The device itself is inherently unstable. It can be installed in an isolated structure between the ground and the isolation level or in between the floors of any fixed and/ or isolated structure. Its effect is that it reduces the forces that are transferred above its installation level.

In order to ensure a considerable amount of positive stiffness around small displacements in order to minimize wind vibrations and account for some variability in structural and NSD properties, a so called gap spring assembly (GSA) mechanism is implemented which essentially makes the device engage at a larger displacement (displacement x_1 in Figure 1) rather than at the initial position of the structure.

The current paper focuses on the analytical framework and experimental validation of the NSD which uses only a part of the experimental NSD testing program. Complete details and additional analytical and computational issues, further experimental validation together with shake table testing and the verification of the true Negative Stiffness (NS) concept through shake table testing can be found in [5, 6].

2 NSD DESCRIPTION

2.1 NSD Operation

The NSD shown in Figure 2a is composed of a pre-compressed spring shown in the center of the device as well the gap spring assemblies on the bottom. A combination of frame elements and plates hold these pieces together. When the device deforms, the pre-compressed spring is the one that creates the force that assists the motion or the negative force and thus the name negative stiffness for the device. The bottom spring assemblies (gap spring assembly mechanism) provide the device inherently with a bilinear elastic positive stiffness in order to make the device engage at larger displacements (displacement x_1 in Figure 1). More specifically, around equilibrium, the positive stiffness caused by the gap spring assembly mechanism, cancels out the negative stiffness caused by the pre-compressed spring so that essentially the force/stiffness generated by the device is close to zero. After a prescribed

displacement, the gap spring assembly softens drastically so that the pre-compressed spring acts essentially on its own creating the negative stiffness. It is noted that the operation of the gap spring assembly is achieved without any yielding so that there is no inherent permanent deformation in the device.

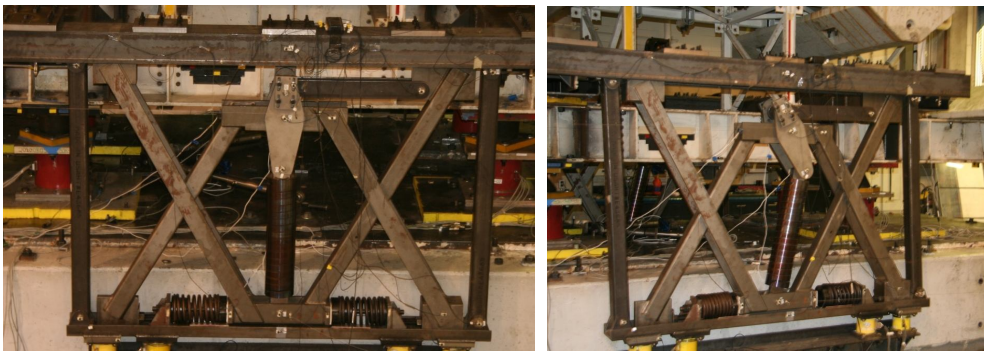

a) Un-deformed NSD b) Deformed NSD

Figure 2: View of Negative Stiffness Device tested at SUNY Buffalo

Schematic diagram of the device in its deformed configuration is shown in Figure 3 after imposing a displacement on the top of the device. The lever imposes a displacement on the top of the pivot plate (point B) making the pivot plate to rotate about point C. Due to the axial rigidity of the lever and its negligible rigid body rotation, the imposed displacement and the displacement of Point B are approximately equal. Since the pivot plate rotates about C, point D moves in the opposite direction from the imposed displacement. Point E is rigidly connected to the top of the device and therefore has a displacement equal to the one imposed. Due to the kinematics of points D and E, the pre-compressed spring rotates and its pre-compression force facilitates the motion rather than opposing it. Moreover since the "negative force" is generated by a spring whose deformation depends nonlinearly to the NSD imposed displacement, the NSD exhibits nonlinear elastic behavior.

The spring exhibits its minimum length when the device is un-deformed. As the device deforms, the spring extends thus its pre-compression force reduces while its inclination angle increases and the stiffness magnitude generated by the device reduces. This gradual stiffness reduction will eventually lead to positive stiffness at larger displacements and this is termed as "stiffening" throughout this paper. This stiffening part can be very important in the case the maximum considered earthquake has been exceeded since it limits the displacements of the structure or the isolators.

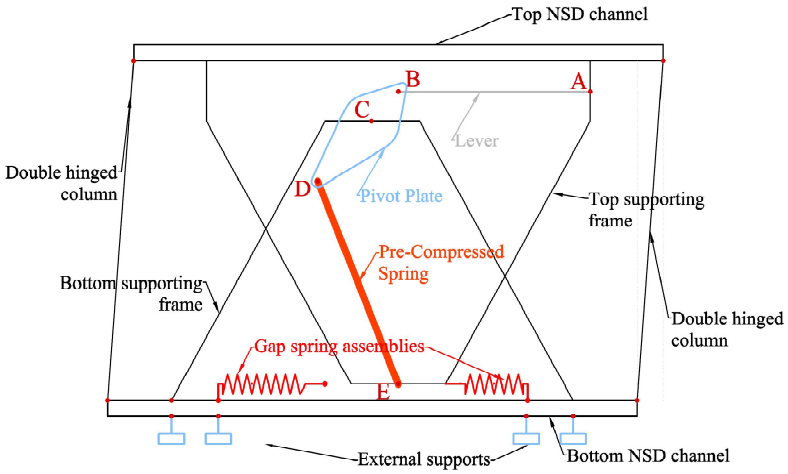

Figure 3: Terminology used for the elements of the Negative Stiffness Device

2.2 Advantages of NSD Tested at SUNY Buffalo

Negative Stiffness in applications other than earthquake has been proposed and used at small scale for the vibration isolation of equipment by Molyneaux (1957) [7], Platus [8-16], Carrella et al [17] and for car suspension systems [18]. It has also been proposed in base isolation [19] with the application of the convex pendulum bearings in parallel with elastomeric bearings. The NSD described in the current paper is a large scale novel design that passively generates negative stiffness and it is not restricted to only base isolation. The NSD presents the following advantages:

- The device changes the **apparent global lateral stiffness** of the structure, without changing the actual stiffness of the structure. The apparent stiffness is reduced to a very low level simulating global lateral yielding without actual yielding in the main structure.
- The device produces **true horizontal negative stiffness** by passively generating a force that assists the imposed displacement. No external power supply is needed since all the elements comprising the device are passive.
- The device is self contained and therefore when installed affects only the horizontal stiffness of the system while leaving the vertical stiffness intact. Stability and buckling limits of the structure are not affected. **The NSD does not participate in transferring the vertical loads.**
- There is no significant hysteresis in the device. The NSD is essentially elastic.
- The device provides variable stiffness which becomes positive at large deformations, therefore its global behavior is “elastic nonlinear”. This is a desired feature as it promotes stability.
- The device employs a double magnification mechanism that allows for easy adjustment of the negative stiffness value. The gap spring assembly (GSA) mechanism allows for adjustable gap opening.

3 OUTLINE OF THE EXPERIMENTAL PROGRAM

The experimental setup is shown in Figure 4a. The 3 story structure –used before as a six story structure [e.g., 20] - is sitting on top of four low damping elastomeric bearings used before in [20]. The elastomeric bearings were tested individually at the single bearing testing machine at UB described in [21]. Two NSD's were installed on the side of the shake table and were connected to the base of the superstructure with rollers in order to accommodate the height loss that they exhibit during deformation. The tests conducted at UB were divided in to two major categories: 1) Displacement controlled tests with and without the gap spring assembly and 2) Shake table tests involving various configurations of the NSD with and without viscous dampers. The displacement controlled tests were achieved by externally bracing the superstructure at the base-mat level through a reaction frame that was constructed on the side of the shake table and shown in Figure 4a on the right while the bracing system is shown in Figure 4b.

a) 3story structure tested at UB b) Bracing of superstructure

Figure 4: Experimental Setup

Each NSD is sitting on top of four load cells [22] and instrumented at points B,C,D,E with string pots and accelerometers. NSD East is also heavily instrumented with Krypton LED's. Krypton is an advanced camera coordinate tracking system described in [23].

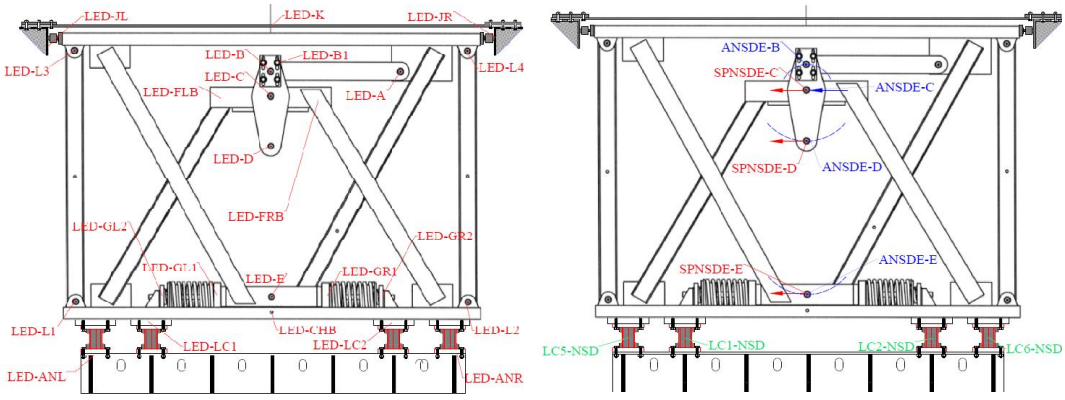

a) Position of LED's on NSD East b) Conventional Instrumentation of NSD East

Figure 5: Instrumentation for NSD East

4 ANALYTICAL EQUATIONS OF NEGATIVE STIFFNESS DEVICE

In order to derive the force displacement equations of the device, equilibrium at the deformed shape needs to be considered since essentially the operation of the device is based on geometric nonlinearity. Therefore one needs to consider the deformed shape and the device being supported horizontally on top by the application of a force which is essentially the negative force generated by the device. The forces acting on the pivot plate caused by the pre-compressed spring and the lever are shown in Figure 6. From geometry and considering the fact that point C is fixed, the displacements of other points of the device are:

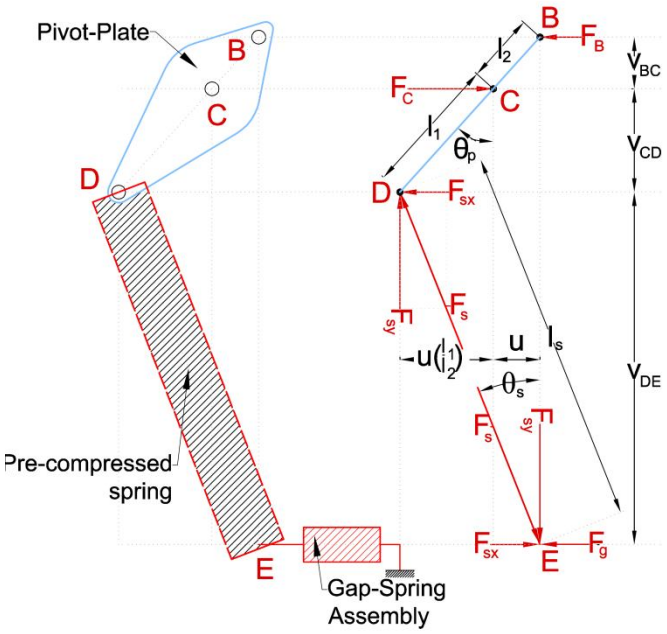

Figure 6: Forces acting on pivot plate

$$u_B = u_E = u_D \, l_2 / l_1 = u \tag{1}$$

In Figure 6, θ_s is the angle of the spring θ_p the angle of the pivot plate with respect to vertical. θ_s and θ_p are obtained from equation (2):

$$\theta_s = \arcsin \frac{1}{l_s} u \left(1 + \frac{l_1}{l_2} \right)$$
$$\theta_p(t) = \arcsin \frac{u}{l_2} \tag{2}$$

The spring length at the deformed configuration is given by:

$$l_s = \sqrt{\left(l_p + l_1 - l_1 \sqrt{1 - \left(\frac{u}{l_2} \right)^2} \right)^2 + u^2 \left(1 + \frac{l_1}{l_2} \right)^2} \tag{3}$$

l_p is the length of the spring when the NSD is un-deformed and F_s is the force of the pre-compressed spring:

$$F_s = P_{in} - K_s\left(l_s - l_p\right) \tag{4}$$

P_{in}: is the pre-compression force of the spring and should have a positive value and K_s is the stiffness of the pre-compressed spring.

Writing the equilibrium equations for the pivot plate for the forces of Figure 6 and using equations (1)-(4) yields the horizontal force at point C. Then from Figure 3 one can see that the total NSD force is simply $F_{NSD} = F_C + F_g$. The final expression for the force generated by the NSD as a function of the imposed displacement is given in equation (5):

$$F_{NSD} = -\left(\frac{P_{in} + K_s l_p}{l_s} - K_s\right)\left(\frac{l_1}{l_2}\right)\left(2 + \frac{l_2}{l_1} + \frac{l_p + l_1}{\sqrt{{l_2}^2 - u^2}}\right)u + F_g \tag{5}$$

The force displacement of the gap spring assembly for monotonic positive displacement is given by:

$$F_g = \begin{Bmatrix} k_{g1}u, & 0 \le u \le d_{gap} \\ k_{g1}d_{gap} + k_{g2}\left(u - d_{gap}\right) & u > d_{gap} \end{Bmatrix} \tag{6}$$

d_{gap} is a prescribed displacement at which the gap spring assembly softens and H is the Heaviside function

Quantity	Value
Distance from spring pin to fixed pin	$l_1 = 10in$
Distance from lever pin to fixed pin	$l_2 = 5in$
Spring length	$l_p = 30in$
Spring rate	$K_s = 0.8\,{kips}/{in}$
Preload	$P_{in} = 3.7kips$
Gap opening	$d_{gap} = 0.65in$
Gap Spring Assembly Stiffness for $u < d_{gap}$	$K_{g,1} = 2.81kips/in$
Secondary spring assembly stiffness $u > d_{gap}$	$K_{g,2} = 0.17kips/in$

Table 1: NSD Properties

The force displacement loops for the derivations above are generated in figure 7 for the properties shown in Table 1.

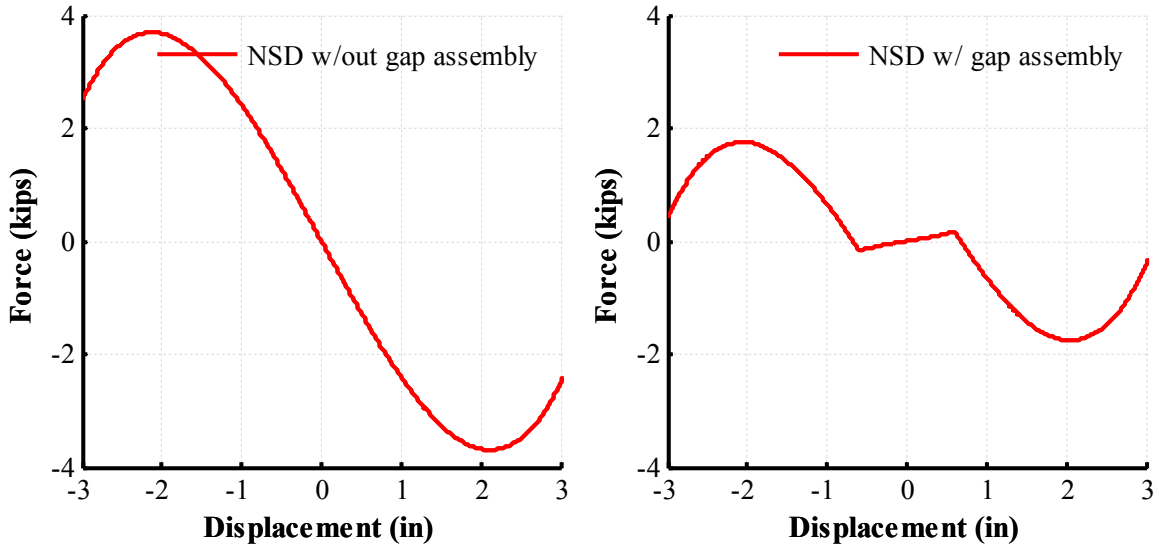

Figure 7: Force versus NSD imposed displacement plots for NSD with and without the gap spring assembly

5 MODELING OF NSD IN SAP2000

Modeling the NSD in user subroutines is straightforward by implementing equations (5) and (6). In SAP2000 [24], the NSD behavior can be modeled using the multi-linear elastic spring element. One can directly import the force displacement loop of the NSD into SAP2000. There is no restriction in SAP2000 for the sign of the stiffness and therefore negative springs can be implemented as well. The gap spring assembly can be also modeled using the same multi-linear element. The NSD model in SAP2000 is therefore a parallel arrangement of two elements 1) a multi- linear elastic element representing the negative nonlinear elastic component from equation (5) with $F_g=0$ and 2) a multi- linear elastic element representing the positive bilinear elastic component generated by the gap spring assembly and given by equation (6).

The configuration as implemented in SAP2000 is shown in Figure 8 on the left. Both elements ML1 and ML2 share the same joints on top and bottom. Comparisons of the results obtained in the SAP2000 model for a displacement controlled test are compared with the analytical equations in Figure 8 on the right. Results match identically.

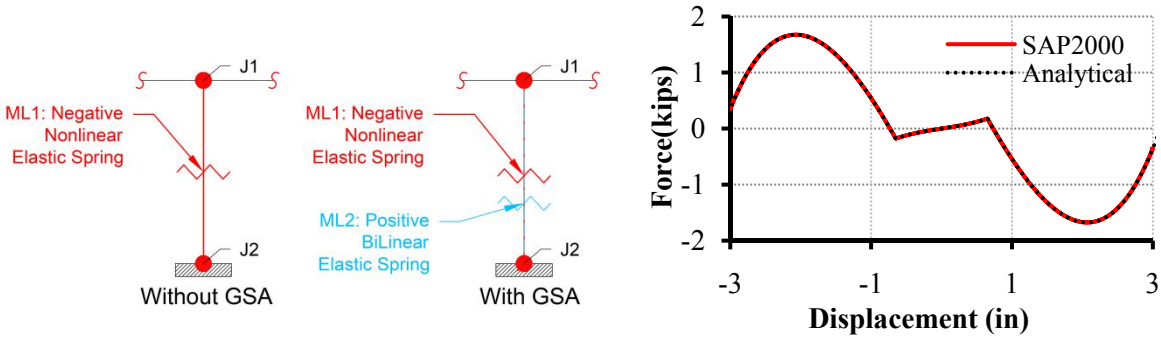

Figure 8: SAP2000 NSD elements for the cases with gap and without gap and comparisons of SAP2000 results with analytical results

6 ANALYTICAL INVESTIGATIONS AND MODELING OF THE DETAILED NSD BEHAVIOR

For most practical applications, the analytical equations and the modeling of sections 4 and 5 is sufficient to provide highly accurate results. The derivations of this section are intended to provide the reader with complete understanding of the detailed mechanics of the NSD. Understanding the complete mechanics of a system is essential in its practical implementation and later on use of the simplified models.

6.1 Analytical Derivations of NSD Dynamics

The rigid body dynamics of the Negative Stiffness are derived here using a Lagrangian formulation. The masses and moments of inertia in the actual device are shown in Figure 9. All frame elements connected to the top channel and the double hinged columns, undergo an inverted pendulum motion around the base and their moment of inertia is lumped at F and H respectively. At point C the mass moment of inertia of the pivot plate is lumped. The center of mass of the spring undergoes both translation and rotation. Its mass m_s is lumped at its center of mass located at point S. Its moment of inertia varies with displacement u.

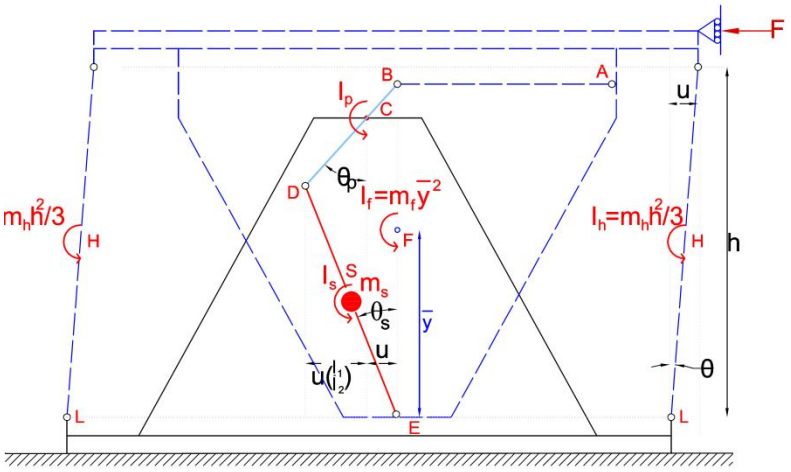

Figure 9: Discretization of the device

Considering the fact that the rotations of the individual components are coupled to the imposed displacement there is only one degree of freedom. The rotation of the pivot plate and spring is given by equation (2), the horizontal displacement of the center of mass of the spring is the average of the displacements of points D and E from equation (1) while the vertical displacement is half the vertical displacement of point D and can be easily calculated from geometry of Figures 3, 6 and 9 while angle θ can be calculated from the geometry of figure 9. All quantities above are functions of the imposed NSD displacement alone.

The Euler-Lagrange equation for the NSD is:

$$\frac{d}{dt}\left(\frac{\partial L}{\partial \dot{u}}\right)-\frac{\partial L}{\partial u}=0 \qquad (7)$$

$$L=K-V$$

Where K is the total kinetic energy of the system and V is the total potential energy of the system with respect to a reference coordinate system given as the sums of the kinetic and

potential energies of the individual moving parts of the device. The total kinetic and potential energies (with reference to C) of the system are given from:

$$K = \frac{1}{2} I_p \dot{\theta}_p{}^2 + \frac{1}{2} m_s \dot{u}_s{}^2 + \frac{1}{2} m_s \dot{v}_s{}^2 + \frac{1}{2} I_s \dot{\theta}_s{}^2 + \frac{1}{2} I_h \dot{\theta}^2 + \frac{1}{2} I_f \dot{\theta}^2$$
$$V = -m_f g\left(l_p + l_1 - \bar{y}\cos\theta\right) - m_s g\left(l_1 + \frac{v_{DE}}{2}\right) + m_c g\left(h - v_{LB} - \frac{h}{2}\cos\theta\right) + V_{el,s} + W \tag{8}$$

The potential energy coming from the deformation of the spring in equation (8) is:

$$V_{el,s} = \frac{1}{2} K_s \left[l_s - \left(l_p + \frac{P_{in}}{K_s} \right) \right]^2 \tag{9}$$

The external work done by a restraining force in (8) has to be expressed as a potential so:

$$W = -\int F du = -Fu + C \tag{10}$$

It is noted that the force above is the force needed to be applied at the top of device in order to hold the device in place and make it stable. Equivalently this is the force generated by the device.

Using equations (7)-(10), (1)- (4) and after performing some tedious algebra which involves the calculation of the derivatives involved in equations (7) and (8) we can get the equation of motion of the NSD which is given by:

$$M_a \ddot{u} + M_v \dot{u}^2 + M_u u = F \tag{11}$$

The terms M_a, M_v and M_u, are given by complex expressions and final results are omitted for simplicity. The force displacement loops of the device for various driving frequencies are plotted in Figure 10 for the device properties of table 1. The effect of the inherent dynamics is that of increasing the negative stiffness and maximum force generated by the NSD while slightly delaying the initiation of stiffening. The driving frequencies of Figure 10 are only for demonstration purposes. The accelerations and velocities for the higher frequencies shown there are unrealistic and therefore the effect of the inherent dynamics is negligible.

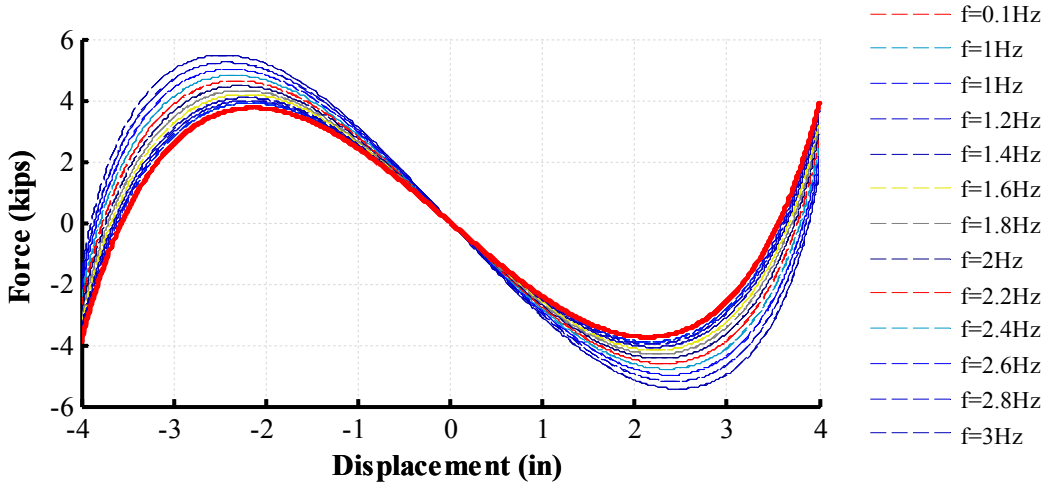

Figure 10: Force Displacement Loops of NSD for various excitation frequencies

6.2 Analytical Derivations of NSD Imperfections

Although the pins are typically assumed to be frictionless and dimensionless, in reality they are not. When a pin is connecting two members, in order for the member to start rotating relatively one to the other, a friction force must be overcome either between one member and the pin, or the other member and the pin, or both. For example consider the assembly shown in Figure 11a:

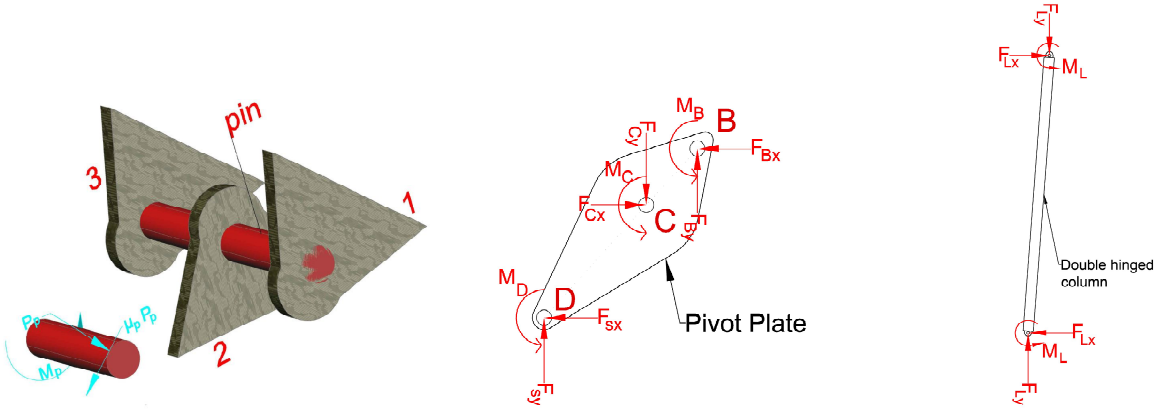

a) Pin Friction modeling FBD

b) Pivot Plate Free body Diagram

c) Double Hinged Column

Figure 11: Pin friction model

In Figure 11a, it is assumed that rotation of the pin occurs because connecting part 1 rotates relatively to the pin while the pin and part 2 are in sticking conditions. In order to have a relative rotation between one of the connecting parts and the pin, we need to apply a torque on the pin of magnitude:

$$M_p = r\mu_p |P_p| \tag{12}$$

r is the radius of the pin, P_p is the resultant force acting on the pin and μ_p is the friction coefficient.

Figure 11b shows the free body diagram of the pivot plate and 11c of the doubled hinged columns considering friction in the pins. Based on Figure 11b, due to the moment at points B and A, the lever now has a shear force equal to:

$$F_{By} = \frac{2M_B}{l_{lv}} \tag{13}$$

Writing the equilibrium equations for Figure 11b the unknown forces can be computed:

$$F_{Bx} = -\frac{F_s}{l_s}\frac{l_1}{l_2}\left[1+\frac{l_p+l_1}{\sqrt{l_2{}^2-u^2}}\right]u + \frac{M_D+M_B+M_C+\frac{2M_B}{l_{lv}}\left(l_2-\sqrt{l_2{}^2-u^2}\right)}{\sqrt{l_2{}^2-u^2}}$$

$$F_{Cx} = F_{Bx} - \frac{F_s}{l_s}u\left(1+\frac{l_1}{l_2}\right) \tag{14}$$

$$F_{Cy} = -F_s\frac{l_p+l_1-\frac{l_1}{l_2}\sqrt{l_2{}^2-u^2}}{l_s} + F_{By}$$

From Figure 11c, the end moments caused by the friction in the pins cause a shear force that is constant throughout the height of the double hinged columns:

$$F_{Lx} = \frac{2M_L}{h} \tag{15}$$

The total force of the NSD becomes:

$$F_{NSD} = F_{Cx} + 2F_{Lx} + F_g \tag{16}$$

The equation above can be decomposed into a nonlinear elastic part and a hysteretic part, $F_{NSD} = F_{el} + F_{pl}$. We approximate the hysteretic moment by using the Sivaselvan-Reinhorn [25] hysteretic model:

$$dM = k_o\left\{1-\left|\frac{M}{M_y}\right|^2 sign(M)sign(d\theta)\right\}d\theta \tag{17}$$

$d\theta$ is the rotation increment of the pin being different for each pin, du is the increment of the imposed displacement while k_o elastic stiffness of the pin prior to slipping occurring.

According to equation (17), in order to calculate the moments of the pins, we need to calculate the resultant forces as well as the rotation increments of all the pins. The resultant forces can be calculated from the free body diagrams of Figure 11b, c. The pin rotation increments can be calculated by differentiating the pin rotations with respect to the imposed NSD displacement and then solving for the rotation differentials. The pin rotations are given from equation (2) for point C, similarly for point B if the negligible rotation of the lever is ignored, as $\theta_D = \theta_C + \theta_s$ for point D with the help of equation (2) for the spring angle and from the geometry of Figure 9 for the rotation θ of the double hinged columns.

The set of equations (12)-(15) and (17) written for each pin with its corresponding resultant forces and rotation increments represent a system of equations on the unknowns. Consider the unknown vector at time step $n+1$:

$$\mathbf{x}_{(n+1)} = \begin{bmatrix} M_{Bn+1} & M_{Cn+1} & M_{Dn+1} & M_{Ln+1} & F_{(n+1)} & F_{Bx(n+1)} & F_{By(n+1)} & F_{Cx(n+1)} & F_{Cy(n+1)} & F_{Lx(n+1)} \end{bmatrix}^T \tag{18}$$

Collecting all terms of the equations on the left hand side and define $\mathbf{f}(\mathbf{x}_{n+1}) = 0$, using $\mathbf{x}_{n+1}{}^{(0)} = \mathbf{x}_n$ as the first iteration, then Newton Raphson iteration follows as:

$$\mathbf{x}_{n+1}^{(j+1)} = \mathbf{x}_{n+1}^{(j)} - D\mathbf{f}^{-1}\left(\mathbf{x}_{n+1}^{(j)}\right) f\left(\mathbf{x}_{n+1}^{(j)}\right) \tag{19}$$

Note that the initial conditions at the first step is $\mathbf{x}_0 = \lfloor 0 \quad 0 \quad 0 \quad 0 \quad 0 \quad 0 \quad 0 \quad 0 \quad P_{in} \quad 0 \rfloor$

Results are plotted in Figure 12 for the properties listed in table 1 for various friction coefficients. Hysteresis in the NSD is proportional to the horizontal force exerted by the NSD. At large displacements when the NSD force becomes zero so does the hysteretic force while after that it maintains the same sign.

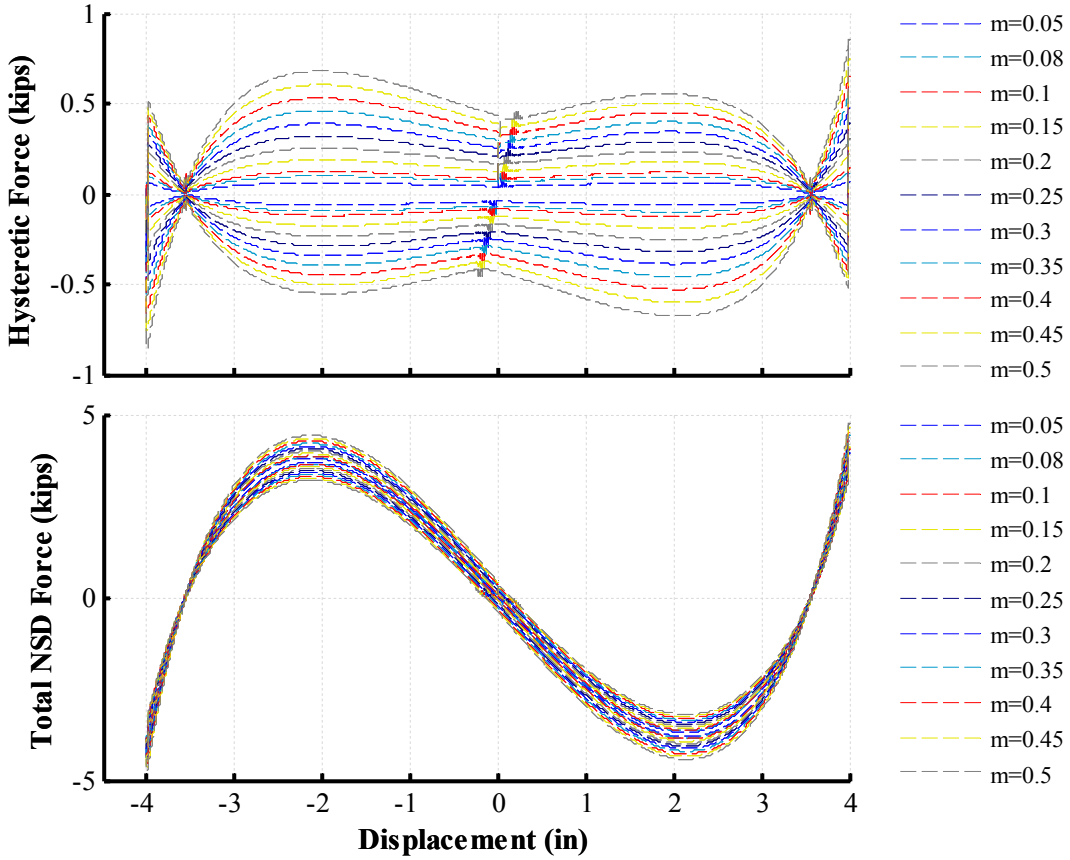

Figure 12: Force Displacement Loops of NSD for various friction coefficients

6.3 Analytical Derivations of NSD Inherent Flexibilities

All the equations up to this point have been derived based on the assumption that point C is fixed and point E undergoes only rigid body motion driven by the top channel of the device. This is only true if the connecting frame elements, namely, the top supporting and the bottom supporting frames are considered rigid. This in most cases is only approximately true.

In order to visualize the flexibility effects, consider an equivalent NSD model shown in Figure 13 in equivalence to the points of Figure 3. Now, at point C a spring k_b is added to approximately represent the flexibilities of the bottom frame together with the bottom supporting channel. Similarly for the top supporting frame, the rigid frame element is no longer assumed to be continuous since a spring k_t is added at its midpoint in order to approximate the flexibilities of the top supporting frame together with the top NSD channel.

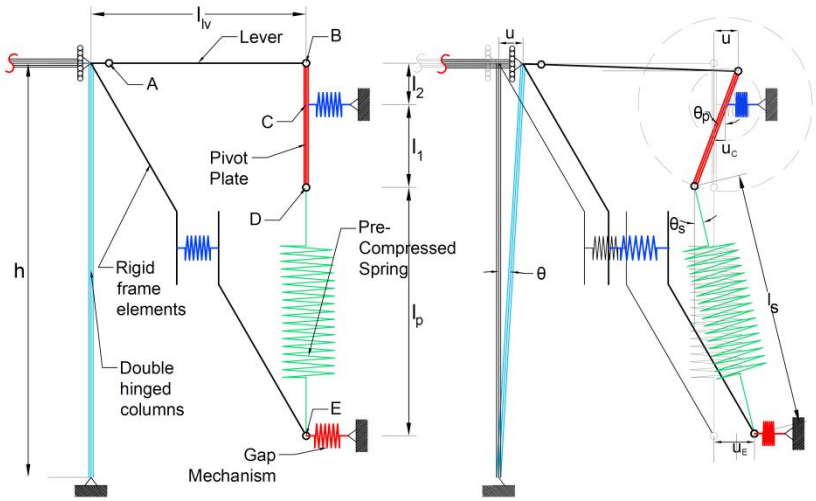

Figure 13: Flexibilities considered in the equivalent NSD model

Equilibrium equations and geometric equations need to be rewritten using equation (20) instead of equation (1):

$$u_{f,E} = u_E - u$$

$$u_D = (u - u_C)\frac{l_1}{l_2} - u_C \tag{20}$$

u_{fE} : Displacement of point E due to flexibilities of the top supporting frame

The spring length is now given from:

$$l_s = \sqrt{\left(l_p + l_1 - \sqrt{{l_1}^2 - \left((u-u_C)\frac{l_1}{l_2}\right)^2}\right)^2 + \left[(u-u_C)\frac{l_1}{l_2} - u_C + u_E\right]^2} \tag{21}$$

The horizontal reaction at point C can be calculated from moment and force equilibrium of the pivot plate for the new geometry:

$$F_{Cx} = -\left(\frac{P_{in} - K_s l_p}{l_s} + K_s\right)\frac{l_1}{l_2}\left\{\left[\frac{(l_p + l_1)}{\sqrt{{l_2}^2 - (u-u_C)^2}} + 1\right](u-u_C) + (u_E - u_C)\left(1 + \frac{l_2}{l_1}\right)\right\} \tag{22}$$

Moreover from equilibrium of forces at point C one gets:

$$F_{Cx} = k_b u_C \tag{23}$$

While from equilibrium of point E after substituting for the spring inclination angle:

$$-\left(\frac{P_{in} + K_s l_p}{l_s} - K_s\right)\left[(u-u_C)\left(\frac{l_1}{l_2}\right) - u_C + u_E\right] + F_g = k_t(u - u_E) \tag{24}$$

The force displacement of the GSA is related to the total displacement of point E and is given for positive displacements from equation (25):

$$F_g = \begin{Bmatrix} k_{g1}u_E, & 0 \le u_E \le d_{gap} \\ k_{g1}d_{gap} + k_{g2}\left(u_E - d_{gap}\right) & u_E > d_{gap} \end{Bmatrix} \tag{25}$$

Then the total NSD force is given from:

$$F_{NSD} = F_{Cx} + F_g \tag{26}$$

Equations (22)-(26) together with the help of (21) and (4) are a system of 5 nonlinear equations on 5 unknowns which are collected in the following vector $\mathbf{x} = \begin{bmatrix} F_{Cx} & F_g & F_{NSD} & u_C & u_{fE} \end{bmatrix}^T$. Then similarly to the hysteresis derivations, all equations are brought on the left hand side, written at step $n+1$ and iterate based on equation (19).

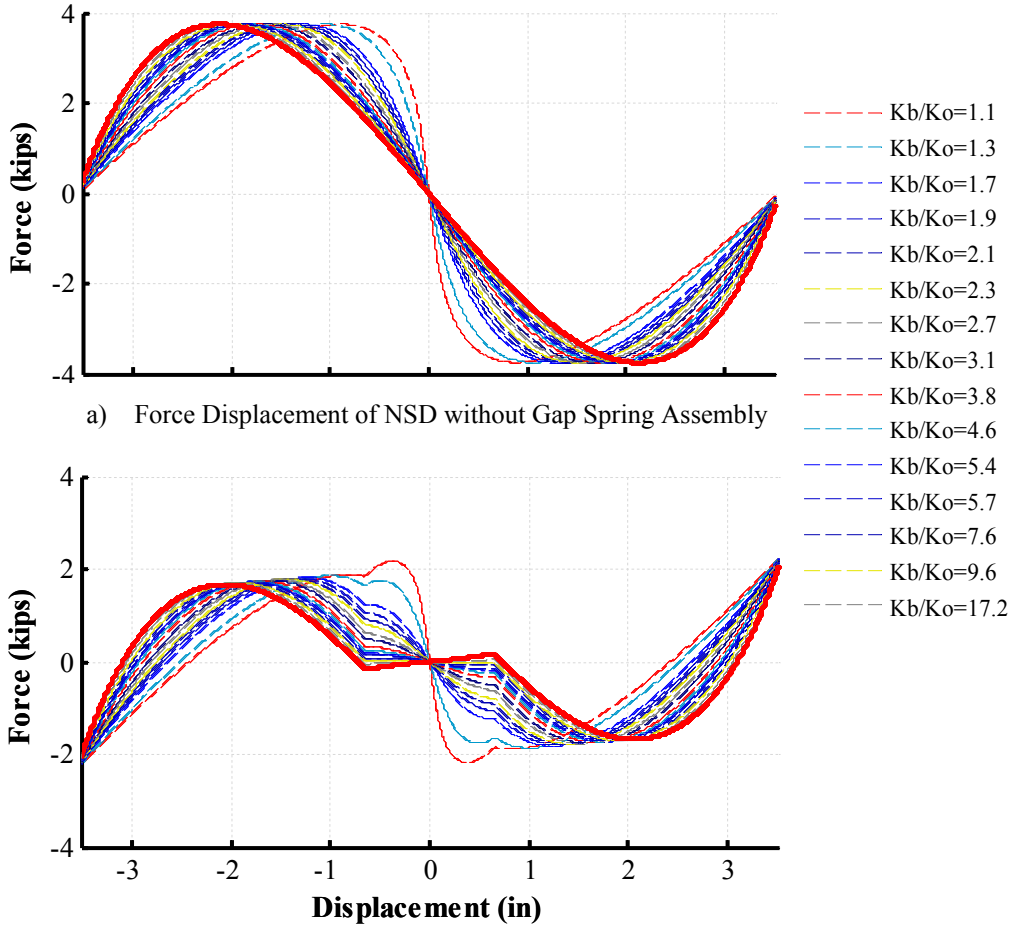

a) Force Displacement of NSD without Gap Spring Assembly

b) Force Displacement of NSD with Gap Spring Assembly

Figure 14: NSD force displacement loops assuming rigid top frame and flexible bottom supporting frame for various stiffness values of the bottom supporting frame

It is noted, that the flexibility of the bottom frame is equivalent to arranging a negative spring in series with a positive spring. Figure 14 shows the results assuming the top frame is rigid and considering various stiffness values for the bottom supporting frame. Legend values are given as ratios of the stiffness of the bottom supporting frame to the Negative NSD stiffness at zero displacement. Flexibility of the bottom frame leads to increased negative stiffness generated by the NSD while the peak force is unchanged and therefore stiffening of the NSD occurs faster than if the bottom frame was rigid. An additional effect of increasing

the Negative Stiffness is the fact the gap spring assembly becomes ineffective since the imposed NSD displacements together with the NSD force becomes inconsistent as shown in Figure 14b.

Results assuming a rigid bottom frame and a flexible top frame are shown in Figure 15a. Due to this flexibility, this case affects the results only when the gap spring assembly is present since point E cannot follow the imposed NSD displacement. This is obvious in Figure 15b which is the force versus NSD imposed displacement of the gap spring assembly.

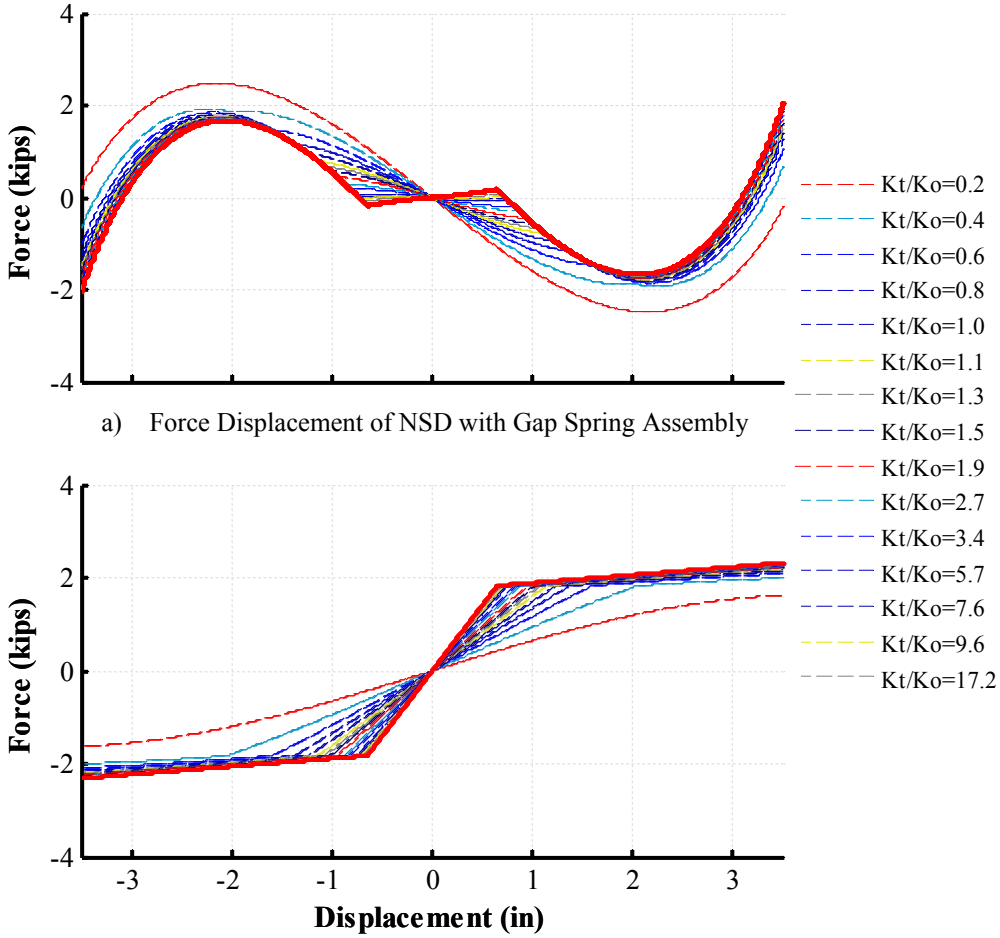

a) Force Displacement of NSD with Gap Spring Assembly

b) Force Displacement of NSD with Gap Spring Assembly

Figure 15: NSD and Gap Spring Assembly force displacement loops assuming rigid bottom and flexible top supporting frame for various stiffness values of the top supporting frame

7 EXPERIMENTAL RESULTS

Results from the experimental study conducted at UB are presented here for the displacement controlled tests. These results are only a minor portion of the complete experimental program. Complete details, additional analytical derivations and results are presented in [5 and 6]. Figure 16 shows the NSD force displacement loops obtained for displacement controlled tests conducted at *0.02Hz* as well as comparisons of the forces obtained from the elastomeric bearings, the NSD's and the total base shear. Installing the Negative stiffness device indeed reduces the total base shear and generates a "negative force" if one compares the red line with the blue line. The blue line represents what the base shear would have been in the absence of the NSD.

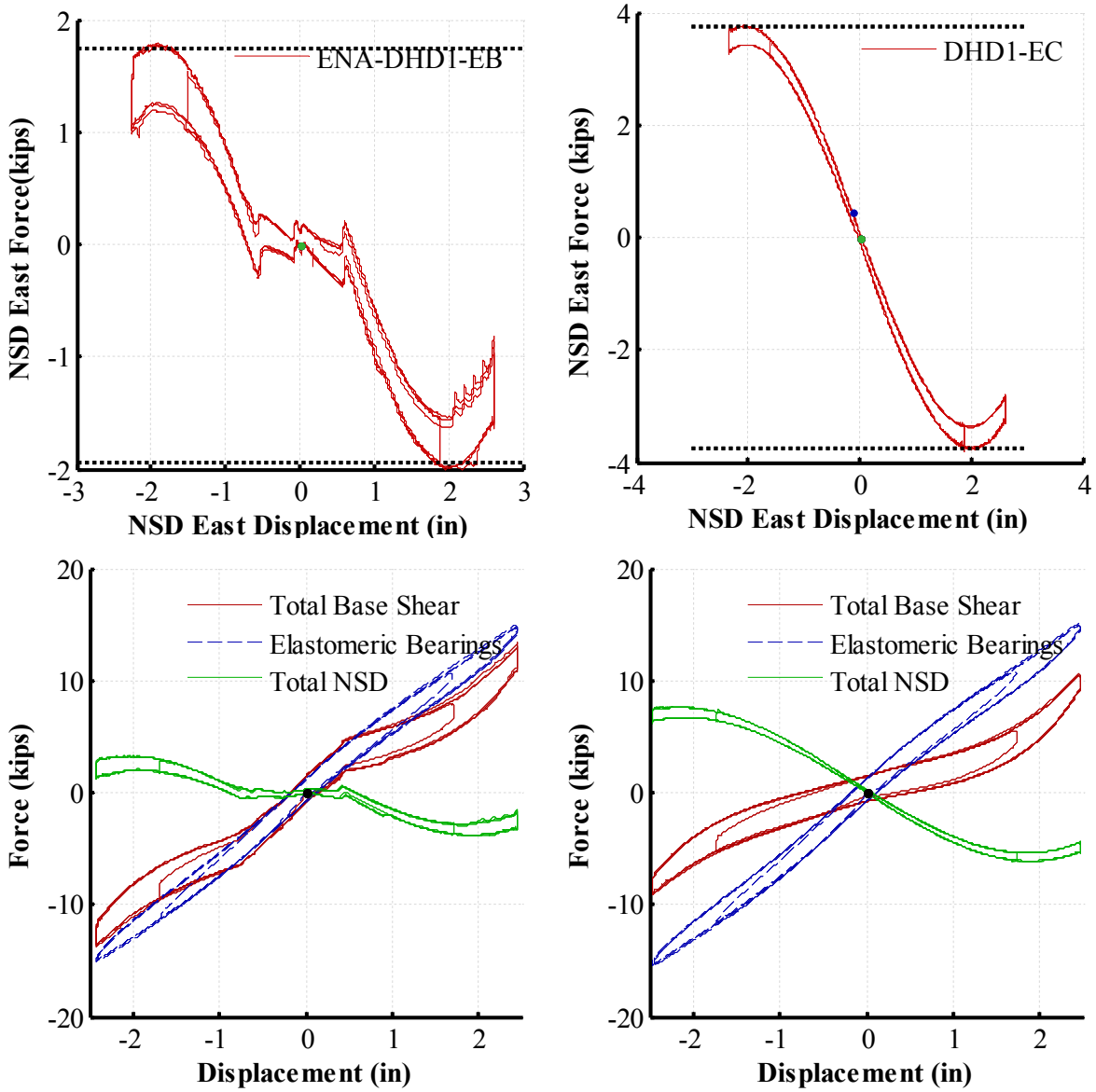

a) With Gap Spring Assembly b) Without Gap Spring Assembly

Figure 16: Experimental Results from Displacement Controlled Tests of NSD

Figure 17 shows the results obtained from Krypton for the most significant points of the NSD. As expected, point A which is the displacement imposed on the NSD, point B and point E have approximately equal displacements while point D is double in magnitude and opposite in sign from the displacement of point B. All displacements below are given as the relative displacements between their absolute displacements and the displacement of the shake table.

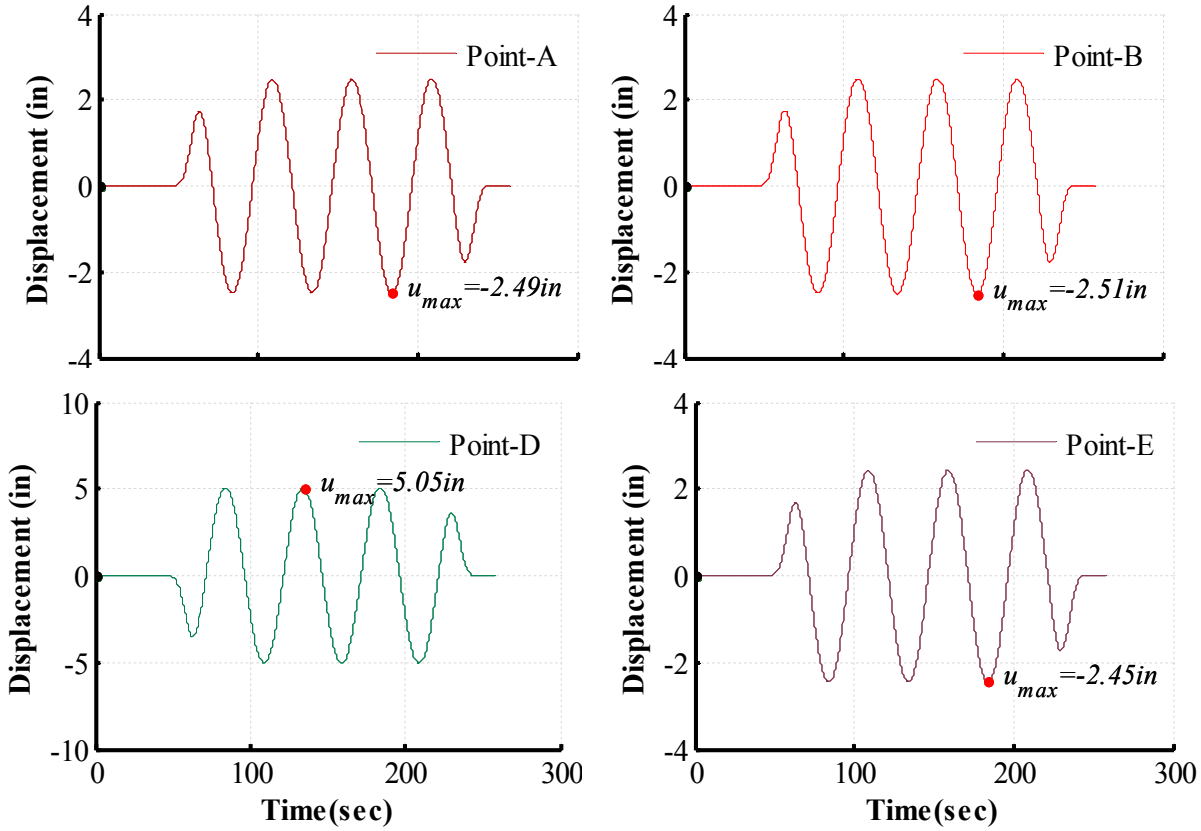

Figure 17: Experimental results from Krypton data acquisition system for displacement controlled tests

8 VERIFICATION OF ANALYTICAL EQUATIONS AND COMPUTATIONAL MODELS

Figure 18 compares all the analytical results described earlier with the results obtained from the experiments. With the exception of the dynamic model comparisons, all other results are shown for static tests conducted at *0.02Hz* frequency. Analytical results are plotted for the nominal properties of table 1 in order to demonstrate the additional advantage that the NSD exhibits of small variability of its properties. The absence of friction elements and the absolute dependence of the NSD behavior on the pre-loaded spring and geometry make the NSD behavior to be predictable at the design level. Note that inclusion of the flexibilities of the top frame explains the smaller stiffness in the gap spring assembly active region- observed in the experimental results- the dynamics explain the higher "negative force observed during the high frequency tests while the hysteretic element accurately follows the hysteresis trend observed in experiments. Based on these comparisons one can though conclude that the basic analytical equations derived in section 3 are sufficient for accurately capturing the NSD behavior assuming proper design was followed.

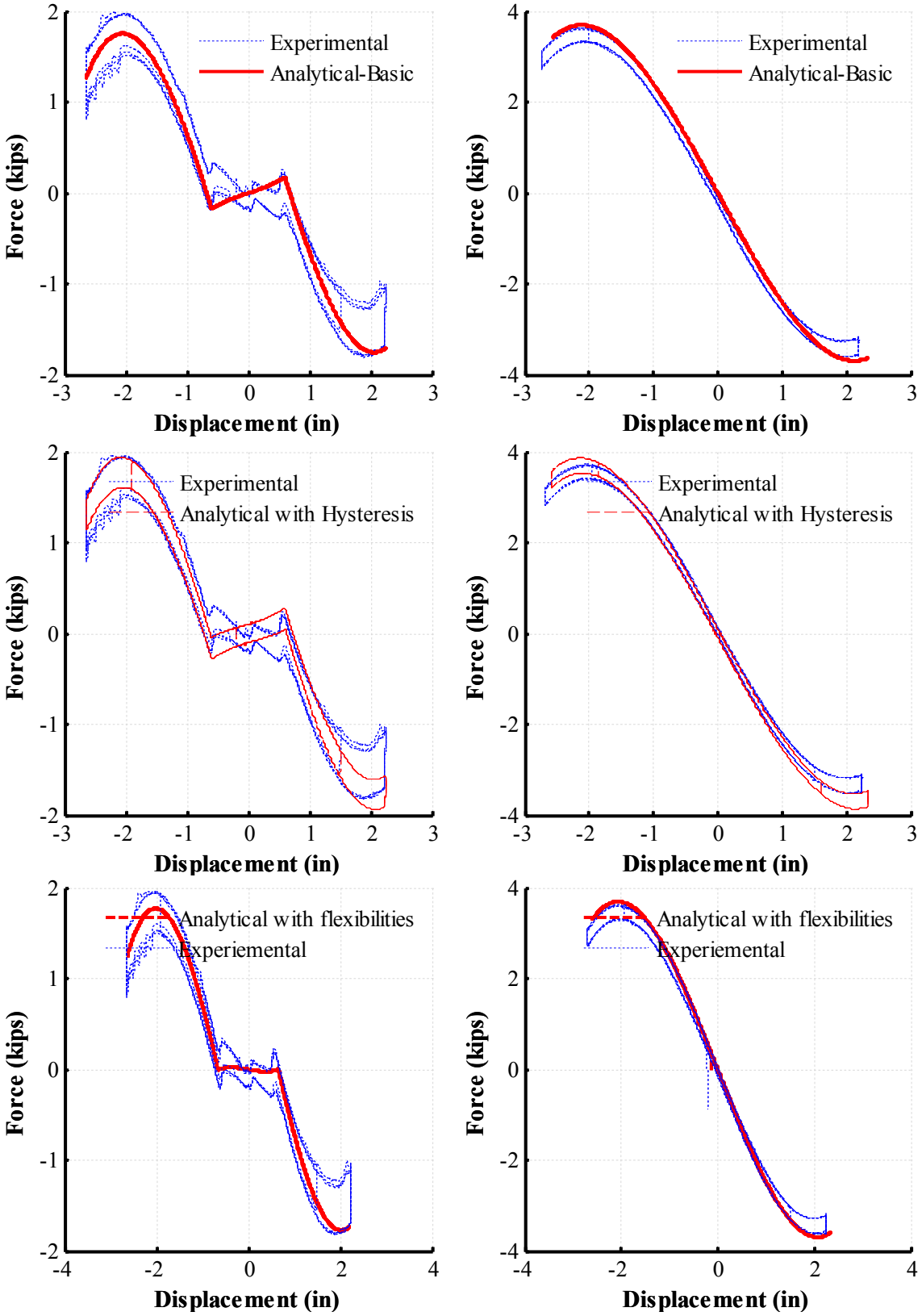
Experimental
Analytical-Basic
Force (kips)
Displacement (in)
Experimental
Analytical-Basic
Force (kips)
Displacement (in)
Experimental
Analytical with Hysteresis
Force (kips)
Displacement (in)
Experimental
Analytical with Hysteresis
Force (kips)
Displacement (in)
Analytical with flexibilities
Experiemental
Force (kips)
Displacement (in)
Analytical with flexibilities
Experiemental
Force (kips)
Displacement (in)

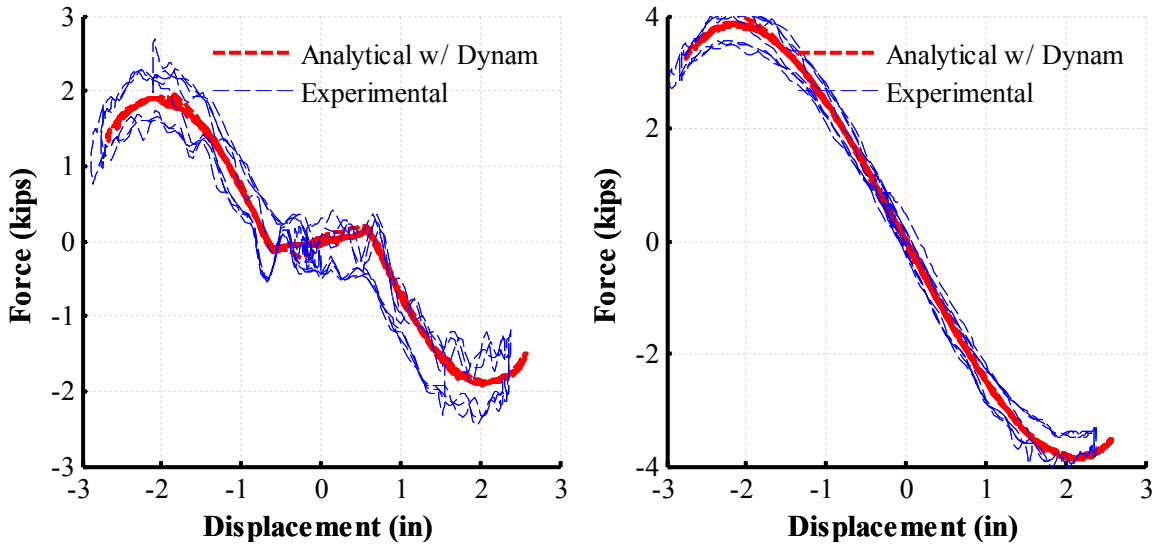

Figure 18: Verification of analytical derivations

9 CONCLUSIONS

Based on the material presented above the following may be concluded:

- A novel Negative Stiffness Device (NSD) has been developed. Proof of concept testing was performed at the NEES facility at the University at Buffalo. The NSD was shown to generate negative stiffness and reduce the base shear of a structure.
- Installing a Negative Stiffness Device is an efficient method of reducing the "apparent strength/stiffness" of a structure's floor/story without affecting the vertical stiffness or stability limits of the structure**.**
- NSD operates with only minor energy dissipation and can be considered to be nonlinear "elastic". Any minor permanent deformations that the NSD might exhibit are eliminated by the gap-spring assembly.
- Basic NSD properties that determine its behavior are adjustable and therefore the NSD can generate a wide range of behaviors by simple adjustments that can be performed even after the installation of the device.
- NSD generates reliable and predictable behavior which can be accurately predicted. This is due to the mechanical nature of the device, consisting of links and springs of well known geometry and of predictable mechanical properties. Note that the comparisons of the analytical versus experimental results are done using the nominal spring properties in order to specifically demonstrate this advantage. No testing was conducted on the individual components (springs).
- Although the NSD behavior might be affected by many factors, the influence of those factors is minor. The NSD behavior can be very accurately predicted by the equations of section 3 and modeling of section 4. Additional complex derivations presented herein help in obtaining understanding of the complete mechanics of the system and provide the designer with additional confidence in using the NSD in practical applications.
- Complete details on the experimental program as well as further analytical and computational work will be enclosed in [5] and [6].

REFERENCES

[1] Reinhorn A.M., Viti S., and Cimellaro G.P. (2005), "Retrofit of Structures: Strength Reduction with damping enhancement.", Proceeding of the 37th UJNR Panel Meeting on Wind and Seismic Effects, Tsukuba, Japan.

[2] Viti S., Cimellaro G. P., and Reinhorn A. M. (2006), Retrofit of a Hospital through Strength Reduction and Enhanced Damping. Smart Structures and Systems, 2(4), 339-355.

[3] Nagarajaiah S., Reinhorn A. M., Constantinou M. C., Taylor D., Pasala, D. T. R. and Sarlis, A. A. (2010), "True Adaptive Negative Stiffness: A New Structural Modification Approach for Seismic Protection". 5th World Conference on Structural Control and Monitoring, Tokyo, Japan, July 12-14.

[4] Iemura H. and Pradono M.H. (2009), "Advances in the development of pseudo-negative-stiffness dampers for seismic response control," Structural Control and Health Monitoring, 16(7-8), 1545-2255.

[5] Sarlis A.A., Constantinou M.C, Reinhorn A.M, Pasala, D.T.R, Nagarajaiah S. and Taylor D. (2011), "Negative Stiffness Device- Part 1: Analytical Framework and Experimental Validation" - MCEER-11-XXXX, Multidisciplinary Center for Earthquake Engineering Research, Buffalo, NY.

[6] Sarlis A.A., Constantinou M.C, Reinhorn A.M, Pasala, D.T.R, Nagarajaiah S. and Taylor D. (2011) , Negative Stiffness Device- Part 2: Shake table testing and Proof of Negative Stiffness Concept" MCEER-11-XXXX, Multidisciplinary Center for Earthquake Engineering Research, Buffalo, NY.

[7] Molyneaux W. G. (1957), "Supports for vibration isolation", ARC/CP-322, Aeronautical Research Council, Great Britain.

[8] Platus D.L., Negative-stiffness-mechanism vibration isolation systems, Proceedings of SPIE—The International Society for Optical Engineering, Vibration Control in Microelectronics, Optics, and Metrology, San Jose, CA, USA, Vol. 1619, 1992, pp. 44–54.

[9] Platus D.L., Negative-stiffness-mechanism vibration isolation systems, Proceedings of the Opto-mechanical Engineering and Vibration Control Conference, SPIE—The International Society for Optical Engineering, Denver, CO, USA, Vol. 3786, 1999, pp. 98–105.

[10] Platus D.L. (1993), "Vibration Isolation System", US Patent No. 5178357, Washington DC: US Patent and Trademark Office.

[11] Platus D.L. (1994), "Vibration Isolation System", US Patent No. 5310157, Washington DC: US Patent and Trademark Office.

[12] Platus D.L. (1994), "Damped Vibration Isolation System", US Patent No. 5370352, Washington DC: US Patent and Trademark Office.

[13] Platus D.L. (1995), "Vibration Isolation System", US Patent No. 5390892, Washington DC: US Patent and Trademark Office.

[14] Platus D.L. and Cunningham P. J (1996), "Vibration Isolation System", US Patent No. 5549270, Washington DC: US Patent and Trademark Office.

[15] Platus D.L. and Durran D.A (1997), "Vibration Isolation System", US Patent No. 5669594, Washington DC: US Patent and Trademark Office.

[16] Platus D.L. (2004), "Vibration Isolation System", US Patent No. 6676101B2, Washington DC: US Patent and Trademark Office.

[17] Carrella A., Brennan M.J., Waters T.P. and Shin K. (2008) On the design of a high-static-low-dynamic stiffness isolator using linear mechanical springs and magnets, Journal of Sound and Vibration, 315(3), 712-720

[18] Lee C. M., V. Goverdovskiy and A. Temnikov (2007), "Design of springs with 'negative' stiffness to improve vehicle driver vibration isolation", Journal of Sound and Vibration 302 (4-5) (2007) 865–874. URL http://dx.doi.org/10.1016/j.jsv.2006.12.024

[19] H. Iemura, O. Kouchiyama, A. Toyooka and I. Shimoda (2008). "Development of the Friction-Based Passive Negative Stiffness Damper and its Verification Tests using Shaking Table".The 14th World Conference on Earthquake Engineering, October 12-17, 2008, Beijing, China

[20] Wolff E.D. and Constantinou M.C. (2004). "Experimental Study of Seismic Isolation Systems with Emphasis on Secondary System Response and Verification of Accuracy of Dynamic Response History Analysis Methods", Technical Report MCEER-04-0001, Multidisciplinary Center for Earthquake Engineering Research, State University of New York at Buffalo, Buffalo, NY, USA.

[21] Kasalanati A. and Constantinou M.C. (1999). "Experimental Study of Bridge Elastomeric and Other Isolation and Energy Dissipation Systems with Emphasis on Uplift Prevention and High Velocity Near Source Seismic Excitation", Technical Report MCEER-99-0004, Multidisciplinary Center for Earthquake Engineering Research, State University of New York at Buffalo, Buffalo, NY, USA

[22] Bracci J.M., Reinhorn A.M. and Mander J.B. (1992). " Seismic Resistance of Reinforced Concrete Frame Structures Designed Only for Gravity Loads: Part I- Design and Properties of a One- Third Scale Model Structure", Technical Report NCEER-92-0027, National Center for Earthquake Engineering Research, State University of New York at Buffalo, Buffalo, NY, USA

[23] Structural Engineering and Earthquake Simulation Laboratory (2004). "Laboratory Manual" SEESL, Buffalo, NY USA. Available online: htto://nees.buffalo.edu/docs/labmanual/html/

[24] Computers and Structures Inc. (2007)."SAP2000: Static and Dynamic Finite Element Analysis of Structures (Version 11.0.2) Analysis Reference Manual", Computers and Structures, Inc., Berkeley

[25] Sivaselvan M.V. and Reinhorn A.M. (2001). "Hysteretic Models for Deteriorating Inelastic Structures", ASCE Journal of Structural Engineering, 126(6) 633-640.